International Journal of Modern Physics C, Vol. 10, No. 8 (1999) 1553–1562

LARGE SCALE LONG-LIVED HETEROGENEITY IN THE DYNAMICS OF SUPERCOOLED LIQUIDS

RYOICHI YAMAMOTO* and AKIRA ONUKI

Department of Physics, Kyoto University, Kyoto 606–8502, Japan
**E-mail*: *ryoichi@ton.scphys.kyoto-u.ac.jp*

Received 16 September 1999

The local mobility of particles in highly supercooled liquids is demonstrated to be spatially heterogeneous on time scales comparable to the structural relaxation time τ_α. The particle motions in the active regions dominantly contribute to the mean square displacement, giving rise to a diffusion constant systematically larger than the Stokes–Einstein value. The diffusion process eventually becomes homogeneous on time scales longer than the life time of the heterogeneity structure ($\sim 3\tau_\alpha$). The heterogeneity structure in the local mobility is very analogous to the critical fluctuation in Ising spin systems with their structure factor being excellently fitted to the Ornstein–Zernike form.

Keywords: Supercooled Liquid; Glass Transition; Kinetic Heterogeneity; Shear Flow; Molecular Dynamics Simulation.

1. Introduction

As liquids are cooled toward the glass transition, dynamics is drastically slowed down,[1−3] while only small changes can be detected in static properties. One of the main goals of theoretical investigations on the glass transition is to identify the mechanism of the drastic slowing-down. To this end, a number of molecular dynamics (MD) simulations has been carried out for supercooled liquids. Several of them have revealed that the dynamics in supercooled liquids are spatially *heterogeneous*.[4−10] In particular, we have examined bond breakage processes among adjacent particle pairs in our MD simulations of two (2D) and three-dimensional (3D) model fluids and found that the broken bonds in an appropriate time interval ($\simeq 0.05\tau_b$, where τ_b is the average bond breakage time) are very analogous to the critical fluctuations in Ising spin systems. To support this picture, the structure factor of the broken bonds can be excellently fitted to the Ornstein–Zernike form.[4,5] The correlation length ξ thus determined increases with decreasing the temperature T and is related to τ_b or the structural α relaxation time τ_α via the dynamic scaling law, $\tau_\alpha \simeq 0.1\tau_b \sim \xi^z$, where $z = 4$ in 2D and $z = 2$ in 3D. The heterogeneity structure in the bond breakage is essentially the same as that in local diffusivity, which we will discuss below.[6]

In a wide range of liquid states, the Stokes–Einstein relation $D\eta a/k_BT = const.$ is confirmed to be satisfied between the translational diffusion constant D of a tagged particle and the viscosity η even when the tagged particle diameter a is of the same order as that of solvent molecules. However, it is known that this relation is systematically violated in fragile supercooled liquids.[2,5,6,11–14] Sillescu *et al.*, observed the power law behavior $D \propto \eta^{-\nu}$ with $\nu \cong 0.75$ at low temperatures.[11] The same tendency has been detected by molecular dynamics simulations in a 3D binary mixture with $N = 500$ particles[13] and in a 2D binary mixture with $N = 1024$.[14] In our 3D simulations with $N = 10^4$, η and D have varied over four decades, and the power law behavior $D \propto \eta^{-0.75}$ has been observed.[5,6] Many authors have attributed the origin of the breakdown to heterogeneous coexistence of relatively active and inactive regions, among which the local diffusion constant is expected to vary significantly.[11,12,15–17] We have demonstrated via MD simulation that the diffusivity of the particles is indeed heterogeneous on time scales comparable to τ_α but becomes homogeneous on time scales much longer than τ_α.

2. The Model and MD Simulations

We performed MD simulations for 2D and 3D binary mixtures composed of two different particle species, 1 and 2, with $N_1 = N_2 = 5000$ particles with the system volume V being fixed. Parameters chosen are mostly common in 2D and 3D. They interact via the soft-core potential $v_{\alpha\beta}(r) = \epsilon(\sigma_{\alpha\beta}/r)^{12}$, where r is the distance between two particles, $\sigma_{\alpha\beta} = (\sigma_\alpha + \sigma_\beta)/2$, and $\alpha, \beta \in 1, 2$. The interaction is truncated at $r = 4.5\sigma_1$ in 2D and $r = 3\sigma_1$ in 3D. The leapfrog algorithm is used to integrate the differential equations with a time step of 0.005τ, where $\tau = (m_1\sigma_1^2/\epsilon)^{1/2}$. The space and time are measured in units of σ_1 and τ. The mass ratio is $m_2/m_1 = 2$, while the size ratio is $\sigma_2/\sigma_1 = 1.4$ in 2D or 1.2 in 3D. This size difference prevents crystallization and produces amorphous states in our systems at low temperatures. We fixed the particle density at $n = 0.8/\sigma_1^d$, where $n = n_1 + n_2$ is the total number density, and d is the space dimensionality. The system linear dimension is $L = 118$ in 2D and $L = 23.2$ in 3D. For $T \geq 0.526$ in 2D and $T \geq 0.267$ in 3D, no appreciable aging (slow equilibration) effect is detected in various quantities such as the pressure or the density time correlation function owing to very long annealing times (2.5×10^5 at $T = 0.267$ in 3D, for example). However, at the lowest temperatures $T = 0.337$ in 2D and $T = 0.234$ in 3D, a small aging effect remains in the density time correlation function.

Our simulations were performed in the absence and presence of shear flow. In the unsheared case ($\dot\gamma = 0$), we performed simulations under the microcanonical (constant energy) condition. However, in the sheared case ($\dot\gamma > 0$), we kept the temperature at a constant using the Gaussian constraint thermostat. Our method of applying shear is as follows: The system was at rest for $t < 0$ for a very long equilibration time and was then sheared for $t > 0$. Here we added the average velocity $\dot\gamma y$ to the velocities of all the particles in the x direction at $t = 0$ and afterwards

maintained the shear flow by using the Lee–Edwards boundary condition.[19,20] Steady states were then realized after a transient time.

3. Results

3.1. *Heterogeneity in configurational rearrangement*

Bonds between neighboring particle pairs are well-defined in supercooled states because the pair correlation functions $g_{\alpha\beta}(r)$ have a sharp peak at $r \simeq \sigma_{\alpha\beta}$. We followed breakage processes of the bonds to investigate local configurational rearrangements which are relevant for the structural (α) relaxation.[4,5] Our definitions of the bonds are as follows: For each atomic configuration given at time t_0, a pair of particles i and j is considered to be bonded if $r_{ij}(t_0) = |\boldsymbol{r}_i(t_0) - \boldsymbol{r}_j(t_0)| \leq A_1\sigma_{\alpha\beta}$, where i and j belong to the species α and β, respectively. We have set $A_1 = 1.1$ for 2D and 1.5 for 3D. After a lapse of time Δt, pairs are regarded to have been broken if $r_{ij}(t_0 + \Delta t) > A_2\sigma_{\alpha\beta}$ with $A_2 = 1.6$ for 2D and 1.5 for 3D. We stress that the results are insensitive to the precise choice of A_1 and A_2 as long as $1 < A_1 < l_2$ and $A_1 \leq A_2 < l_2$, where l_2 is the second peak position of $g_{\alpha\beta}(r)$ divided by $\sigma_{\alpha\beta}$. We have followed the relaxation of the total surviving (unbroken) bonds $N_{\rm bond}(\Delta t)$ with increasing Δt. No significant difference has been found among the three kinds of bonds, 1–1, 1–2, and 2–2, so we consider the total sum only. We define the bond breakage time τ_b by fitting $N_{\rm bond}(\Delta t)$ to the stretched exponential form, $N_{\rm bond}(\Delta t) \sim \exp[-(\Delta t/\tau_b)^{a'}]$, the exponent a' is close to 1 at relatively high temperatures but is considerably smaller than 1 at the lowest temperatures (for example, $a' \sim 0.6$ at $T = 0.234$ in 3D). Following the bond breakage process, we can visualize the kinetic heterogeneity without ambiguity and quantitatively characterize the heterogeneous patterns. We found the broken bonds in a time interval ($0.05\tau_b$ or $0.1\tau_b$ in our case) are seen to form *clusters* with a characteristic size ξ which increases with decreasing temperature. Furthermore, the clusters of the broken bonds in the subsequent time intervals are found to migrate and eventually cover the whole space. This demonstrates that *active regions* follow complex space-time evolution on the scales of ξ and τ_b. It is worth nothing that this is an important difference between the present structural glass and the spin glass. On the other hand, in shear flow, the heterogeneity is found to become much suppressed, while its spatial anisotropy remains small.

We then defined the structure factor $S_b(q, \Delta t)$ of the broken bonds as

$$S_b(q, \Delta t) = \frac{1}{N_b}\left\langle \left| \sum_{<i,j>} \exp(i\boldsymbol{q} \cdot \boldsymbol{R}_{ij}) \right|^2 \right\rangle, \tag{1}$$

where N_b is the total number of the broken bonds in a time interval $[t_0, t_0+\Delta t]$, and $\boldsymbol{R}_{ij} = (1/2)[\boldsymbol{r}_i(t_0) + \boldsymbol{r}_j(t_0)]$ is the center position of the broken pairs at the initial time t_0, The summation is over the broken pairs, and the angular average over the direction of the wave vector has been taken. We here choose $\Delta t = 0.05\tau_b$ and found

that $S_b(q, 0.05\tau_b)$ can be nicely fitted to the Ornstein–Zernike (OZ) form:

$$S_b(q, 0.05\tau_b) = S_b(0, 0.05\tau_b)/(1 + \xi^2 q^2)\,. \tag{2}$$

The correlation length ξ is determined from this expression. It grows up to the system length at the lowest temperatures and is insensitive to the width of the time interval Δt as long as it is considerably shorter than the bond breakage time τ_b. The agreement of our $S_b(q, 0.05\tau_b)$ with the OZ form can be clearly seen in the plots of $S_b(q, 0.05\tau_b)/S_b(0, 0.05\tau_b)$ versus $q\xi$ in Fig. 1, in which all the data collapse onto a single OZ master curve both in 2D and 3D. In particular, in 3D the deviations are very small, although $\xi \sim L$ for low T and small $\dot{\gamma}$ in our case. We also notice that $S_b(q, 0.05\tau_b)$ is insensitive to the temperature at large q, so from the OZ form, we find

$$S_b(0, 0.05\tau_b) \sim \xi^2\,. \tag{3}$$

The clusters of the broken bonds are thus very analogous to the the critical fluctuations in Ising spin systems. In fact, small-scale heterogeneities with sizes ℓ in the region $1 \ll \ell \ll \xi$ are insensitive to the temperature. The relation (3) is analogous to the relation $\chi \propto \xi^{2-\eta}$ in Ising spin systems between the magnetic susceptibility $\chi = \lim_{q\to 0} S(q)$ and the correlation length ξ near the critical point. Here $S(q)$ is the spin structure factor and η is the Fisher critical exponent ($\ll 1$ in 3D). From our data, we cannot conclude any divergence of ξ at a nonzero temperature, because of the finite-size effect arising from $\xi \sim L$. Furthermore, as in critical dynamics, we have confirmed a dynamical scaling relation between the bond breakage time τ_b and the correlation length ξ,

$$\tau_b \propto \xi^z\,, \tag{4}$$

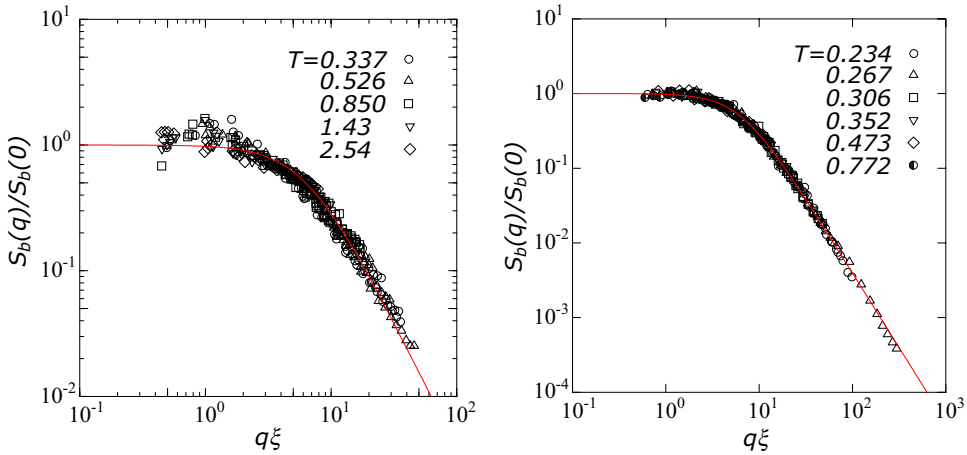

(a) (b)

Fig. 1. $S_b(q, 0.05\tau_b)/S_b(0, 0.05\tau_b)$ on logarithmic scales for various T and $\dot{\gamma}$ in 2D (a) and 3D (b). The solid line is the Ornstein-Zernike form $1/(1 + x^2)$ with $x = q\xi$.

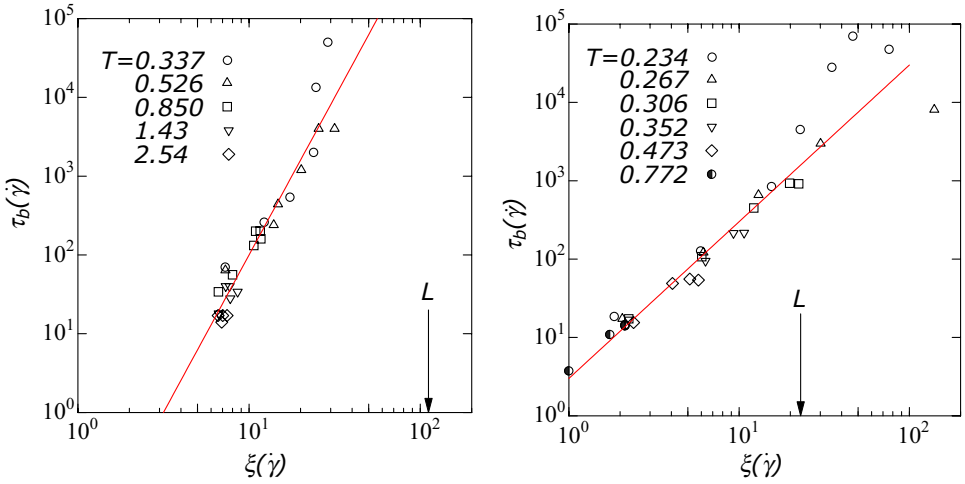

(a) (b)

Fig. 2. Universal relation between the correlation length $\xi(\dot\gamma)$ and the bond breakage time $\tau_b(\dot\gamma)$. In 2D (a), the line of the slope 4 is a viewing guide and L is the system length. The corresponding 3D plot is shown in (b) with the slope being 2.

where $z = 4$ in 2D and $z = 2$ in 3D as shown in Figs. 2(a) and 2(b). At present, we cannot explain the origin of these simple numbers for z. We may only argue that z should be larger in 2D than in 3D because of stronger configurational restrictions in 2D. It is surprising that Eq. (4) holds even in strong shear $\dot\gamma\tau_b(0) \gg 1$. In a zeroth-order approximation, therefore, the kinetic heterogeneities are characterized by a single parameter, ξ or τ_b, owing to the small space anisotropy induced by shear in our systems. The shear rate $\dot\gamma$ is apparently playing a role similar to a magnetic field h in Ising spin systems. Thus, $\dot\gamma$ and T are two relevant external parameters in supercooled liquids, while h and the reduced temperature $(T - T_c)/T_c$ are two relevant scaling fields in Ising systems.

3.2. *Tagged particle diffusion and heterogeneity in local diffusivity*

Let us consider the incoherent density correlation function,

$$F_s(q,t) = \frac{1}{N_1}\left\langle \sum_{j=1}^{N_1} \exp\left[i\boldsymbol{q}\cdot\Delta\boldsymbol{r}_j(t)\right]\right\rangle \tag{5}$$

for the particle species 1, where $\Delta\boldsymbol{r}_j(t) = \boldsymbol{r}_j(t) - \boldsymbol{r}_j(0)$ is the displacement vector of the jth particle. The α relaxation time τ_α is then defined by $F_s(q,\tau_\alpha) = e^{-1}$ at $q = 2\pi$ for various T. We also calculate the coherent time correlation function, $S_{11}(q,t) = \langle n_1(\boldsymbol{q},t)n_1(-\boldsymbol{q},0)\rangle$, where $n_1(\boldsymbol{q},t) = \sum_{j=1}^{N_1}\exp\left[i\boldsymbol{q}\cdot\boldsymbol{r}_j(t)\right]$ is the Fourier component of the density fluctuations of the particle species 1. The decay profiles of $S_{11}(q,t)$ at its first peak wave number $q = q_m \simeq 2\pi$ and $F_s(q,t)$ at $q = 2\pi$

nearly coincide in the whole time region studied ($t < 2 \times 10^5$) within 5%, hence $S_{11}(q_m, \tau_\alpha)/S_{11}(q_m, 0) \cong e^{-1}$ holds for any T in our simulation. Such agreement is not obtained for other wave numbers, however. Furthermore, some neutron-spin-echo experiments[21] showed that the decay time of $S_{11}(q_m, t)$ is nearly equal to the stress relaxation time and as a result the viscosity η is of order τ_α. In agreement with this experimental result, we obtained a simple linear relation $\tau_\alpha \cong (A_\eta/q_m^2)\eta/T$ in our simulations.[6] The coefficient A_η is close to 2π in our system. Here, we may define a q-dependent relaxation time τ_q by $F(q, \tau_q) = e^{-1}$. Thus, particularly at the peak wave number $q = q_m$, the effective diffusion constant defined by $D_q \equiv 1/q^2\tau_q$ is given by the Stokes–Einstein form even in highly supercooled liquids. However, notice that the usual diffusion constant is the long wavelength limit, $D = \lim_{q\to 0} D_q$. It is usually calculated from the mean square displacement, $\langle(\Delta \boldsymbol{r}(t))^2\rangle = \langle\sum_{j=1}^{N_1}(\Delta \boldsymbol{r}_j(t))^2\rangle/N_1$. The crossover of this quantity from the plateau behavior arising from motions in transient cages to the diffusion behavior $6Dt$ has been found to take place around $t \sim 0.1\tau_\alpha (\simeq 0.01\tau_b)$.[5] In Fig. 3(a), we plot $D\tau_\alpha$ versus τ_α, which demonstrates breakdown of the Stokes–Einstein relation in agreement with the experimental trend.[11,12]

To examine the diffusion process in more detail, we consider the van Hove self-correlation function, $G_s(r, t) = \langle\sum_{j=1}^{N_1}\delta(\Delta \boldsymbol{r}_j(t) - \boldsymbol{r})\rangle/N_1$. Then,

$$F_s(q, t) = \int_0^\infty dr \frac{\sin(qr)}{qr} 4\pi r^2 G_s(r, t) \tag{6}$$

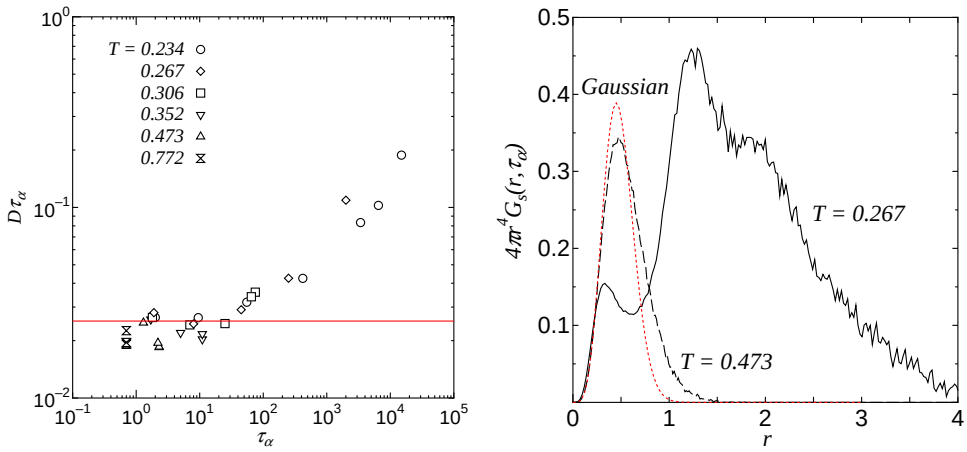

(a) (b)

Fig. 3. (a) $D\tau_\alpha$ versus τ_α in a quiescent supercooled liquid. The solid line represents the Stokes-Einstein value $D_{SE}\tau_\alpha = (2\pi)^{-2}$. (b) $4\pi r^4 G_s(r, t)$ versus r at $t = \tau_\alpha$. The solid line is for $T = 0.267$ and the broken line is for $T = 0.473$. The dotted line represents the Brownian motion result. The peaks at $r \simeq 1.2$ and 2 in the solid line arise from hopping processes in our system at $T = 0.267$. Note that the areas below the curves give $6D\tau_\alpha$.

is the 3D Fourier transformation of $G_s(r,t)$. At the peak wavenumber $q = 2\pi$, the integrand in Eq. (6) vanishes at $r = 1$, and the integral in the region $r < 1$ is confirmed to dominantly determine the decay of $F_s(2\pi,t)$. On the other hand, the mean square displacement

$$\langle(\Delta \boldsymbol{r}(t))^2\rangle = \int_0^\infty dr 4\pi r^4 G_s(r,t) \tag{7}$$

is determined by the particle motions out of the cages for $t \gtrsim \tau_\alpha$ in glassy states. In Fig. 3(b), we display $4\pi r^4 G_s(r,\tau_\alpha)$ versus r, where $\tau_\alpha = 3.2$ and 2000 for $T = 0.473$ and 0.267, respectively. These curves may be compared with the Gaussian (Brownian) result, $(2/\pi)^{1/2}\ell^{-3}r^4\exp(-r^2/2\ell^2)$, where $3\ell^2 = 6D_{SE}\tau_\alpha = 3/2\pi^2$ is the Stokes–Einstein mean square displacement. Because the areas below the curves give $6D\tau_\alpha$, we recognize that the particle motions over large distances $r > 1$ are much enhanced at low T, leading to the violation of the Stokes–Einstein relation.

We then visualize the heterogeneity of the local diffusivity. To this end, we pick up mobile particles of the species 1 with $|\Delta \boldsymbol{r}_j(t))| > \ell_c$ in a time interval $[t_0, t_0 + t]$ and number them as $j = 1,\ldots,N_m$. Here ℓ_c is defined such that the sum of $\Delta \boldsymbol{r}_j(t)^2$ of the mobile particles is 66% of the total sum ($\cong 6DtN_1$ for $t \gtrsim 0.1\tau_\alpha$). In Fig. 4, these particles are drawn as spheres with radii $a_j(t) \equiv |\Delta \boldsymbol{r}_j(t)|/\sqrt{\langle(\Delta \boldsymbol{r}(t))\rangle}$ located at $\boldsymbol{R}_j(t) \equiv (1/2)[\boldsymbol{r}_j(t_0) + \boldsymbol{r}_j(t_0 + t)]$ in time intervals $[t_0, t_0 + \tau_\alpha]$ for $T = 0.473$ (a) and 0.267 (b) and in $[t_0, t_0 + 10\tau_\alpha]$ for $T = 0.267$ (c). The mobile particle number N_m is 1595 in (a), 725 in (b), and 1316 in (c), while the Gaussian results should be $N_m = 1800$. The ratio of the second moments $c_2 \equiv \sum_{j=1}^{N_m} a_j(t)^2 / \sum_{j=1}^{N_1} a_j(t)^2$ is held fixed at 0.66, while the ratio of the fourth moments $c_4 \equiv \sum_{j=1}^{N_m} a_j(t)^4 / \sum_{j=1}^{N_1} a_j(t)^4$ turns out to be close to 1 as $c_4 = 0.89$ in (a), 0.92 in (b), and 0.90 in (c). The mobile particles are homogeneously distributed for $T = 0.473$ at τ_α, whereas for $T = 0.267$, the heterogeneity is significant at τ_α, but is much decreased at $10\tau_\alpha$. In fact, the variance defined by $\mathcal{V} \equiv N_m \sum_{j=1}^{N_m} a_j(t)^4 / (\sum_{j=1}^{N_m} a_j(t)^2)^2 - 1$ is 0.27 in (a),

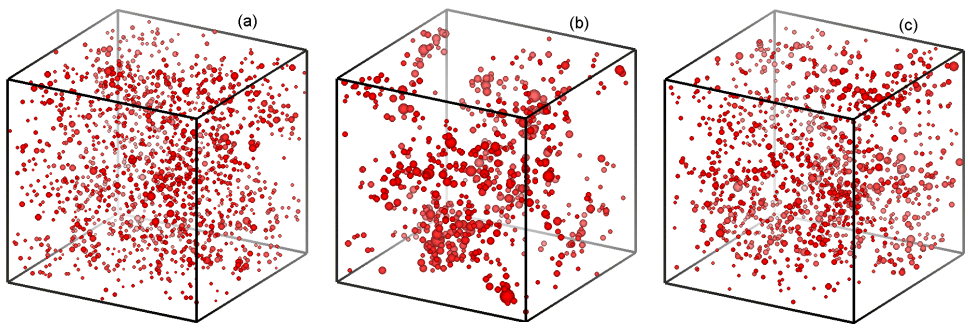

Fig. 4. Mobile particles of the species 1 with a time interval $t = \tau_\alpha$ at $T = 0.473$ (a) and $T = 0.267$ (b) and with $t = 10\tau_\alpha$ at $T = 0.267$ (c). The radii of the spheres are $|\Delta \boldsymbol{r}_j(t)|/\sqrt{\langle(\Delta \boldsymbol{r}(t))^2\rangle}$ and the centers are at $(1/2)[\boldsymbol{r}_j(t_0) + \boldsymbol{r}_j(t_0 + t)]$. The system linear dimension is $L = 23.2$. The darkness of the spheres represents the depth in the 3D space.

0.41 in (b), and 0.32 in (c). Note that the statistical average of $\mathcal{V}$ (taken over many initial times t_0) is related to the non-Gaussian parameter,

$$A_2 \equiv \frac{3\langle \Delta \boldsymbol{r}(t)^4\rangle}{5\langle \Delta \boldsymbol{r}(t)^2\rangle^2} - 1 = \frac{3N_1 \left\langle \sum_{j=1}^{N_1} a_j(t)^4 \right\rangle}{5\left(\left\langle \sum_{j=1}^{N_1} a_j(t)^2 \right\rangle \right)^2} - 1\,, \tag{8}$$

by

$$\langle \mathcal{V}\rangle \cong \frac{5\langle c_4\rangle\langle N_m\rangle}{3c_2^2 N_1}(1 + A_2(t)) - 1\,, \tag{9}$$

where the deviations $c_4 - \langle c_4\rangle$ and $N_m/\langle N_m\rangle - 1$ are confirmed to be very small for large N_1 and are thus neglected. We may also conclude that the significant increase of $A_2(t)$ in glassy states originates from the heterogeneity in accord with some experimental interpretations.[22]

We next consider the Fourier component of the *diffusivity* density defined by

$$\mathcal{D}_{\boldsymbol{q}}(t_0, t) \equiv \sum_{j=1}^{N_1} a_j(t)^2 \exp[-i\boldsymbol{q}\cdot \boldsymbol{R}_j(t)]\,, \tag{10}$$

which depends on the initial time t_0 and the final time $t_0 + t$. The correlation function

$$S_{\mathcal{D}}(q, t, \tau) = \langle \mathcal{D}_{\boldsymbol{q}}(t_0 + \tau, t)\mathcal{D}_{-\boldsymbol{q}}(t_0, t)\rangle / N_1 \tag{11}$$

is then obtained after averaging over many initial states. We plot $S_{\mathcal{D}}(q, \tau_\alpha, 0)$ in Fig. 5(a). The increase in $S_{\mathcal{D}}(q, \tau_\alpha, 0)$ for large q at low T is attributed to increase

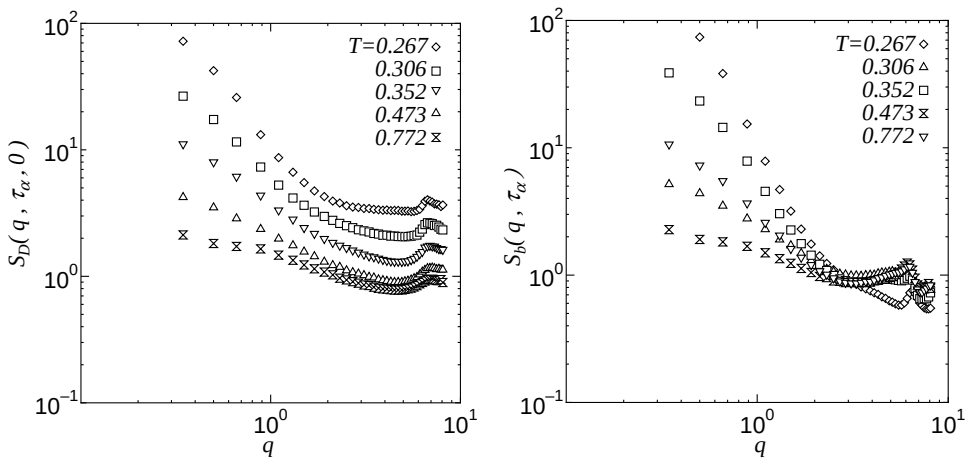

(a) (b)

Fig. 5. The correlation functions (a) $S_{\mathcal{D}}(q, \tau_\alpha, 0)$ and (b) $S_b(q, \tau_\alpha)$.

in $A_2(\tau_\alpha)$. The heterogeneity structure of the broken bonds $S_b(q, \tau_\alpha)$ is also plotted in Fig. 5(b). It is confirmed that $S_{\mathcal{D}}(q, \tau_\alpha, 0)$ tends to its long wavelength limit for $q \lesssim \xi^{-1}$, where ξ coincides with the correlation length obtained from $S_b(q, \tau_\alpha)$.

As the difference τ of the initial times increases with fixed $t = \tau_\alpha$, $S_{\mathcal{D}}(q, \tau_\alpha, \tau)$ relaxes as $\exp[-(\tau/\tau_h(q))^c]$, where $\tau_h(q)$ is the wavenumber dependent life time of the heterogeneity structure. At $T = 0.267$ and $q = 0.345$, we obtained $c \simeq 0.5$ and $\tau_h(q) \simeq 3\tau_\alpha$. The two-time correlation function among the broken bond density also relaxes with τ_h in the same manner.[23]

4. Conclusion

We performed extensive MD simulations and identified *weakly bonded* or *relatively active* regions from breakage of appropriately defined bonds.[4,5] We also found that the spatial distributions of such regions resemble the critical fluctuations in Ising spin systems, so the correlation length ξ can be determined. It grows up to the system size as T is lowered, but no divergence seems to exist at nonzero temperatures. In the present work, we have demonstrated that the diffusivity in supercooled liquids is spatially heterogeneous on time scales shorter than $3\tau_\alpha$, which leads to the breakdown of the Stokes–Einstein relation.[6] The heterogeneity detected is essentially the same as that of the bond breakage in our previous works.

Acknowledgment

This work is supported by a Grant in Aid for Scientific Research from the Ministry of Education, Science, Sports and Culture of Japan. Calculations have been carried out at the Supercomputer Laboratory, Institute for Chemical Research, Kyoto University and the Human Genome Center, Institute of Medical Science, University of Tokyo.

References

1. J. Jäckle, *Rep. Prog. Phys.* **49**, 171 (1986).
2. M. D. Ediger, C. A. Angell, and R. Nagel, *J. Phys. Chem.* **100**, 13200 (1996).
3. M. Tokuyama and I. Oppenheim (eds.), *Slow Dynamics in Complex Systems*, AIP Conference series 469, (AIP, New York, 1999).
4. R. Yamamoto and A. Onuki, *J. Phys. Soc. Jpn.* **66**, 2545 (1997); *Europhys. Lett.* **40**, 61 (1997); A. Onuki and R. Yamamoto, *J. Non-Cryst. Solids* **235–237**, 34 (1998).
5. R. Yamamoto and A. Onuki, *Phys. Rev. E* **58**, 3515 (1998).
6. R. Yamamoto and A. Onuki, *Phys. Rev. Lett.* **81**, 4915 (1998); Ref. 3, p. 476.
7. T. Muranaka and Y. Hiwatari, *Phys. Rev. E* **51**, R2735 (1995); *J. Phys. Soc. Jpn.* **67**, 1982 (1998).
8. D. N. Perera and P. Harrowell, *Phys. Rev. E* **54**, 1652 (1996); D. N. Perera, *J. Phys. Condens. Matter* **10**, 10115 (1998).
9. W. Kob *et al.*, *Phys. Rev. Lett.* **79**, 2827 (1997); S. Glotzer and C. Donati, *J. Phys. Condens. Matter* **11**, A285 (1999).
10. C. Donati *et al.*, *Phys. Rev. Lett.* **80**, 2338 (1998).

11. F. Fujara, B. Geil, H. Sillescu, and G. Fleischer, *Z. Phys. B* **88**, 195 (1992); I. Chang *et al.*, *J. Non-Cryst. Solids* **172–174**, 248 (1994).
12. M. T. Cicerone, F. R. Blackburn, and M. D. Ediger, *Macromolecules* **28**, 8224 (1995); M. T. Cicerone and M. D. Ediger, *J. Chem. Phys.* **104**, 7210 (1996).
13. D. Thirumalai and R. D. Mountain, *Phys. Rev. E* **47**, 479 (1993).
14. D. Perera and P. Harrowell, *Phys. Rev. Lett.* **81**, 120 (1998).
15. F. H. Stillinger and A. Hodgdon, *Phys. Rev. E* **50**, 2064 (1994).
16. G. Tarjus and D. Kivelson, *J. Chem. Phys.* **103**, 3071 (1995).
17. C. Z.-W. Liu and I. Oppenheim, *Phys. Rev. E* **53**, 799 (1996).
18. B. Bernu, Y. Hiwatari, and J. P. Hansen, *J. Phys. C* **18**, L371 (1985); B. Bernu, J. P. Hansen, Y. Hiwatari, and G. Pastore, *Phys. Rev. A* **36**, 4891 (1987); J. Matsui, T. Odagaki, and Y. Hiwatari, *Phys. Rev. Lett.* **73**, 2452 (1994).
19. M. P. Allen and D. J. Tildesley, *Computer Simulation of Liquids* (Clarendon, Oxford, 1987).
20. D. J. Evans and G. P. Morriss, *Statistical Mechanics of Nonequilibrium Liquids* (Academic, New York, 1990).
21. F. Mezei, W. Knaak, and B. Farago, *Phys. Rev. Lett.* **58**, 571 (1987); D. Richter, R. Frick, and B. Farago, *Phys. Rev. Lett.* **61**, 2465 (1988).
22. R. Zorn, *Phys. Rev. B* **55**, 6249 (1997); T. Kanaya, I. Tsukushi, and K. Kaji, Supplement to *Prog. Theor. Phys.* **126**, 133 (1997).
23. R. Yamamoto and A. Onuki, to be published.